# Optical Imaging for Understanding of Thermal Barrier Coated Piston Engine Performance

Chad Koci<sup>1</sup>, Kenth Svensson<sup>1</sup>, Glen Martin<sup>1</sup>, Charlie Kim<sup>1</sup>, Patrick Seiler<sup>1</sup>, Felipe Caliari<sup>2</sup>, John Saputo<sup>2</sup>, Sanjay Sampath<sup>2</sup>

<sup>1</sup>Caterpillar Inc. – Technical Center, 14009 N Old Galena Road, Chillicothe, IL 61523, USA

E-mail: koci\_chad@cat.com Telephone: +(1) 309 675 6747

<sup>2</sup>Center for Thermal Spray Research, Stony Brook University – Stony Brook, NY 11794, USA

E-mail: felipe.caliari@stonybrook.edu

Telephone: +(1) 631 632 9512

Abstract. Thermal barrier coatings (TBC) applied to pistons have been a recently renewed research topic in the field of internal combustion engines. Single cylinder testing of a conventional C15™ Tier 4 final production steel piston and a TBC coated piston showed that the Yttrium stabilized Zirconia (YSZ) TBC did not significantly alter engine performance, with the TBC piston having slower combustion rates and higher criteria emissions. For deeper understanding, research continued by studying 3D-piston sections optically in a constant pressure vessel using photodiodes, four high-speed cameras (natural luminosity, CH\*, and OH\*), and visualization of the flame from two orthogonal directions. Particle Imaging Velocimetry (PIV) algorithms were adapted to perform Combustion Imaging Velocimetry (CIV) to aid in quantification of the observed visual combustion flow field differences. The optical work showed that the TBC piston flame development is slower, spatially different, with lower mixing energy for the TBC variant. Geometric profiles of engine pistons and optical vessel 3D-piston sections were measured using a Coordinate Measurement Machine (CMM), and surface roughness was measured with a stylus surface profilometer. CMM results showed that the TBC piston bowl had reasonable macroscopic accuracy, but the rim had a larger radius with less re-entrancy. A discussion of the results and analyses in relation to future TBC effort and direction concludes the work.

#### 1. Introduction

Thermal barrier coatings (TBC) for internal combustion engines have been a topic of interest for many decades, with work dating back to the 1970's. The motivation for this was clearly reduced fuel consumption and potentially higher engine power density, enabled by the ability to achieve higher working temperatures while adhering to the same substrate temperature limits. A renewed interest was spurred by the work of Kosaka et al. [1] from Toyota Motor Company and a burst of research continued for the coming decade. The TBC review paper by Uchida et al. [2] provides an excellent overview of the TBC efforts to circa 2020 and ends with key steps surrounding measurements of detailed TBC surface temperature, spatial variation understanding, physical property measurements including the impact of deposits, and performing measurements without intrusive disturbance to the temperature field – all of these are challenging endeavours.

The primary assumption of the modern TBC efforts focuses on the idea of a rapidly changing surface temperature to reduce the temperature difference and reduce convective heat flux between the in-cylinder gases and the combustion chamber surfaces. This is attempted through alteration of the combustion chamber surface with a TBC which has low thermal effusivity  $e = \sqrt{kC_p\rho}$  (where k is thermal conductivity,  $C_p$  is specific heat and density is  $\rho$ ). Significant development of the initial TBC concepts utilizing a silica-reinforced porous anodized aluminum "SiRPA" showed promising results in reducing heat transfer and increasing engine efficiency at moderate loads [3]. This work also highlighted the detrimental impact of the elevated coating surface roughness on heat transfer, combustion, and flame development through imaging of spray impingement on a flat surface in a rapid compression machine. Kawaguchi et al. [4] furthered the importance and understanding of the detrimental roughness impact

and found that only coating the top of the piston crown, where there is much reduced spray-wall interaction, produced superior efficiency results. The authors also extended this to the importance of a TBC for cold-start benefits in reduced NOx and fuel consumption attributed to lower heat transfer and therefore lower fuelling required to idle the engine under minimal or idle loads. These results have significant relevance to engines with aluminum pistons but have a disconnect with heavy-duty engines utilizing steel alloys, typically used for temperature limit and strength improvements.

Research on a heavy-duty steel piston coated with a YSZ thermal sprayed TBC by Binder et al. [5] provided data on surface temperature using a 10 Hz phosphor lifetime thermometry technique with a 2-9  $\mu$ m phosphor coating thickness. The work concluded that the maximum surface temperature variations between the steel and TBC piston were similar. Heat flux was reduced for the TBC piston due an elevated mean surface temperature; however, the resulting heat release was slower for the TBC piston and the net efficiency was reduced from the steel baseline. Limitations on the 10 Hz diagnostic forced an ensemble averaging and fitting approach to the temperature data. Recent diagnostic developments from Witkowski and Rothamer [6] may be a way to extend these types of surface temperature experiments to the kHz regime for high-precision individual cycle resolution, and spatial surface temperature mapping. Additionally, the assumption of the non-intrusiveness of ~1-10  $\mu$ m thick phosphor coatings may need re-examining for measurements on steel/metal surfaces since the effusivity of these phosphors are similar to TBC coatings, and therefore may be only well matched for TBC surfaces.

Andrie et al. [7] used newly developed non-thermal spray coatings, with very low effusivity, in a premixed SI engine application and found successes with +1% absolute brake efficiency improvements. This very different combustion application, from a diesel mixing-controlled system with strong spray-wall interaction, indicates promise for the temperature swing concept to be realized with significant impact. A counter point to this is the finding that a permeable porous TBC used in a pre-mixed SI application by Andruskiewicz et al. [8] brought alternate combustion and efficiency loss pathways, highlighting significant problems with porosity and pre-mixed fuel. Additional recent SI application TBC research showed that increased wall temperature reduced the flame quenching distance and actually increased heat flux Hazhizume et al. [9], only very thin (<0.1mm) coatings with low conductivity and specific heat do not suffer from excessive charge heating, and only small efficiency benefit ranges (0.1-0.3%) were identified with a minor impact of TBC surface roughness on heat transfer and combustion Broatch et al. [10, 11].

Other TBC piston relevant works include those of Gingrich et al. [12], where only smoothed thermal sprayed TBC pistons showed efficiency benefits, and Somhorst et al. [13] where a robust statistical testing and analysis found no efficiency benefits with detriments attributed to increased TBC surface roughness. On the topic of TBC durability, Koustakis et al. [14] developed a TBC elastic strain energy mechanics model for coating delamination prediction following prior work on an analytical solution to unsteady heat conduction in TBC applications [15]. A recent work from Kawaharazuka et al. [16] showed high promise by utilizing an alternate approach to create a rapidly changing piston surface temperature without detrimental increases in roughness. A highly polished stainless steel piston bowl was produced with a YSZ TBC on the under-crown cooling gallery. This novel heat insulation increased efficiency by ~1% (56.1 to 56.8% ITE) at an extremely high cylinder pressure and already very efficient operating point. The authors additionally point out the importance of the outstanding convective insulation properties of soot layers, which develop on combustion chamber surfaces, and the high radiative absorption of soot which may allow a rapid and large surface temperature swing. The authors noted increased efficiency the longer the engine was run, with further soot layer accumulation.

The many renewed attempts at TBC application to a mixing controlled diesel combustion system have been challenged by many aspects. Unclear surface temperature and heat transfer phenomena, fluid dynamic and boundary layer changes imposed by surface roughness changes, slowed combustion rates, unclear impacts of exposed porosity, and the precise role of soot deposits in heat transfer are the major aspects of interest. For improved TBC performance and industry adoption, the following are some suggested areas of needed focus:

- Overcoming surface roughness increases from TBC materials and application methods
- Understanding combustion system intrusiveness of the TBC application
- Validating the coating durability
- Quantifying the role of soot deposits, exposed porosity, and temporal evolution
- Measuring 3D spatial impacts on local heat transfer

Improving the coating process accuracy and cost for complex diesel piston geometries

This work attempts to add some insight into the changes TBC surfaces impose on a heavy duty mixing controlled combustion system using single cylinder engine testing and a 3D piston combustion vessel optical diagnostic.

### 2. Experimental Setup

For the TBC efforts within this experimental setup the thermal properties of the coating layers were measured using a commercially available (DXF 900, TA Instruments, New Castle, DE, USA) standardized thermal flash method (ref ASTM E1461) along with Archimedes principle and a precision mass balance. Thermal diffusivity and specific heat were simultaneously measured using the former technique and used along with density measured through the latter to calculate thermal conductivity, taken as the product of the three directly measured variables.

The coatings used were derivatives of TBCs used in gas turbines. A NiCrAI based "bond-coat" alloy (443NS, Oerlikon-Metco, Westbury, NY, USA) was applied directly to the component to increase adhesion of the ceramic TBC, grade the transition of thermal and mechanical properties, and aid in oxidation resistance. Afterwards an insulating Yttria-Stabilized Zirconia "top-coat" layer (SG204, Saint-Gobain Coating Solutions, Worcester, MA, USA) toughened with the inclusion of 5% volume of the metallic bond-coat phase was applied. Table 1 lists the nominal material properties relevant to the coating and piston efforts, while

Table 2 lists average piston combustion bowl surface roughness as measured by a 1D stylus surface profilometer and are averages of measurements over two different azimuthal locations for each bowl radial location. A clear increase for the TBC pistons can be seen and is in the range from 2-5 µm Ra, which is rougher than the steel pistons but in the same range as other reported piston TBC attempts [12,13].

Layer	Material	Thickness mm	Conductivity W/m-k	Density kg/m <sup>3</sup>	Vol. Heat Capacity kJ/m <sup>3</sup> -K	Thermal Effusivity W-s <sup>0.5</sup> /m <sup>2</sup> -K
Bond Coating	NiCrAl	0.100	4.85	7120	2814	3694
TBC Topcoat	95/5% YSZ/NiCrAl	0.225	0.91	5299	1864	1299
Steel	4140	N/A	43.4	7850	3423	12187
Stainless Steel	304	N/A	16.2	8000	4000	8050

**Table 1**. Material and nominal properties at 300K reference temperature

Table 2. Piston Surface Roughness, Ra

Component	Material	Center µm	Bowl µm	Chamfer µm	Crown µm
SS Optical-Piston	Stainless Steel	1.2	1.1	0.8	0.6
Steel Piston	Steel	1.7	1.3	1.0	1.2
TBC Optical-Piston	Polished TBC Topcoat	2.1	2.2	4.6	3.1
TBC Piston	Polished TBC Topcoat	2.2	5.3	3.4	4.8

# 2.1 TBC Application Process

A direct current (DC) argon-hydrogen air plasma spray (APS) process (F4MB, Oerlikon-Metco, Westbury, NY, USA) configured with a 6 mm nozzle and a 90° 1.8 mm injector was used to fabricate all coatings described in this work. Before deposition, all surfaces were degreased and grit blasted at 80 psi from a 125 mm distance using 24 mesh alumina grit. Primary and secondary gas flow rates were held at 45 and 6 NLMP with a current setpoint of 550 A operating at 57 V. Carrier gas flow rates were set between 2.5 and 4 NLMP for the bond and top-coat layers and were optimized on a per-run basis to ensure consistent deposition between components.

Coatings on both optical-piston sections and C15™ Tier 4 piston crowns were produced by traversing the spray torch along the component centerline normal to the crown geometry while rotating the component. To ensure microstructural uniformity and aid in the control of thickness buildup the surface velocity was kept uniform as the torch moved towards the component center. This was

accomplished through trial and error by varying both the rotational speed of the component and the torches traverse speed. To aid in rapid toolpath development mock component geometries were produced that could be easily attached to the crown of a production piston. These mock geometry components could then quickly be destructively tested to confirm the coating uniformity. This process is shown schematically in Fig. 1. The same optimized toolpath was then used to deposit coatings on the optical-piston sections by fixturing them in a manned identical to the production pistons.

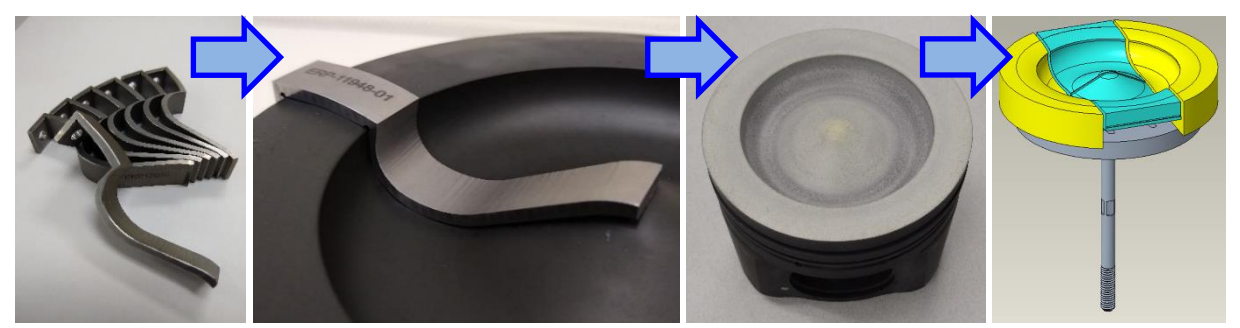


Fig. 1. TBC application process utilizing profile strips for spray setup and ease analysis

#### 2.2 Single Cylinder Test Engine

The experimental methodology for the present work centered on Single Cylinder Test Engine (SCTE) experiments. A heavy-duty diesel SCTE platform was used based on a Cat® C15 $^{\text{TM}}$  (15 L) production engine, but with a modified cylinder head, valvetrain, and fuel injection system. The geometric specification for the engine is listed in Table 3 with a nominal displacement of 2.5 L/cylinder.

	SCTE
Displaced volume	2.53 L
Bore	137.19 mm
Stroke	171.45 mm
Connecting Rod	270.76 mm
Compression Ratio (nominal)	16.9:1
Piston Bowl Shape	Conventional Open
Valves	4-valve
Swirl Level	< 1 Swirl Number
Valve Train	DOHC
Fuel Injector	Common Rail: 7-hole/258 µm / 130° SA / 4.9 kg/min

 $\textbf{Table 3.} \ Single \ Cylinder \ Test \ Engine \ Nominal \ Specifications$ 

The engine was coupled to a General Electric DC Motoring Dynamometer. Torque was measured at the end of a 21" arm using an Artech 90515 load cell. A central low speed data acquisition system was used to interface between all instrumentation in the single cylinder laboratory and recorded temperature, pressure, flow, and emissions measurements at 1 Hz. An AVL Indicom high speed data acquisition system provided crank angle resolved cylinder pressure, intake manifold pressure, exhaust manifold pressure, and engine speed. The encoder resolution was 0.1 crank angle degrees (CAD). Cylinder pressure was measured with a Kistler 6125C piezoelectric transducer connected to an AVL Micro IFEM charge amplifier that used a 100 kHz low pass digital filter and cyclic drift compensation. Kistler 4045a piezoresistive transducers were used to measure intake and exhaust manifold pressures. 200 consecutive cycles of high speed data were recorded at each data point.

A schematic of the single-cylinder engine laboratory is shown in Fig. 2. The engine air handling system allows for complete control of the intake pressure, intake temperature, and exhaust pressure. A Horiba MEXA 7100 DEGR was used to measure gaseous emissions including NO, NO<sub>2</sub>, CO, total hydrocarbons (THC), O<sub>2</sub>, intake CO<sub>2</sub> and exhaust CO<sub>2</sub>. Particulate emissions were measured with an AVL 415S smoke meter.

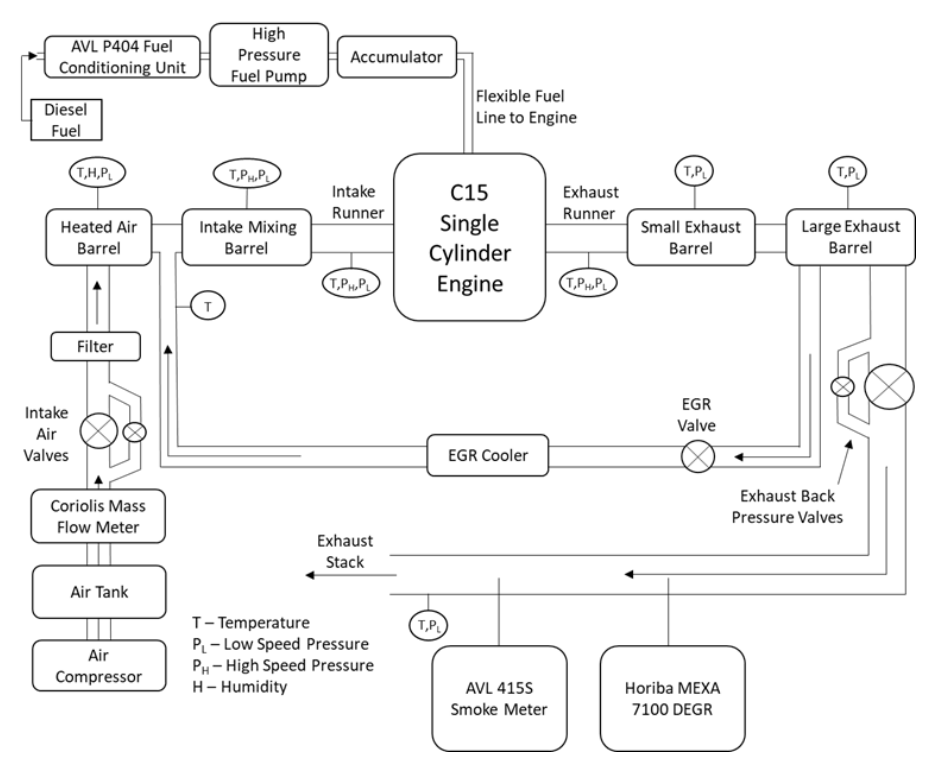


Fig. 2. Schematic of Single Cylinder Engine Laboratory

The experimental pistons were measured using a coordinate measuring machine for specific interest in the resulting bowl profile shape. Fig. 3 overlays the profiles between the optical TBC, single cylinder test engine TBC, and production steel piston in the left of the figure. The right inset plot compares the optical steel and TBC profiles to the target production piston. The macroscopic bowl profile shape is good, while there is notable deviation at the corner with the TBC variants having less reentrancy and more rounding. The challenge of thermal spray TBC bowl accuracy was noted by Binder et al. [5], and the present work looks to be improved despite the remaining inaccuracies. The impact of this deviation on combustion and emissions performance will be discussed in the results sections.

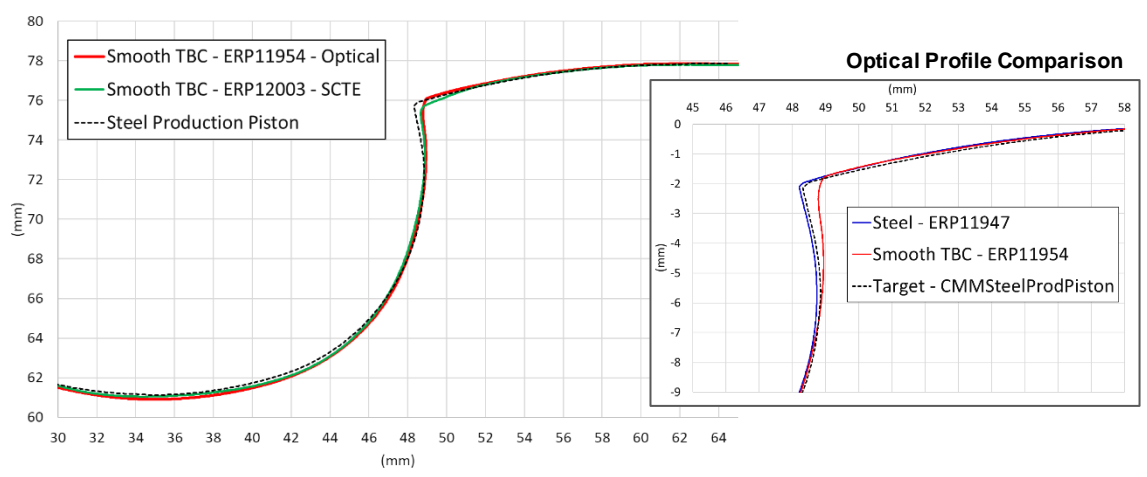


Fig. 3. Coordinate Measuring Machine piston bowl profile comparison plots showing the steel and TBC differences between the SCTE and the optical vessel

## 2.3 High Temperature Pressure Vessel

Designed to enable repeated observation of fuel sprays, the High Temperature Pressure Vessel (HTPV) employed in this work can reach steady pressures of 150 bar and temperatures of 1100 K uniformly across the inner core of the test section [17]. 3D piston sections were mounted in the HTPV to enable study of the combusting fuel jet interaction with both production-similar and TBC coated surfaces. This setup shown in Fig. 4, enabled orienting the fuel-jet relative to the piston bowl to match the 130° included angle utilized in engine testing [18]. Utilizing an on-axis single-orifice injector tip required holding the piston section base with a 25° angled block. The overall 3D piston section optical setup includes a flat fused-silica window to represent a simplified cylinder-head surface. The stainless plate that holds the window also simulates the crevice volume above the top piston ring, see Fig. 5. The 3D piston section was sized to represent geometry equivalent to a C15 engine fitted with a 6-hole injector tip. Two linear adjustments allow for sliding the 3D piston section away from the injector tip while simultaneously maintaining the injector to cylinder head offset. This allows for setting the equivalent crankangle positioning of the 3D piston section. For the current study the 3D section is offset by 2 mm to simulate a 10 CAD BTDC/ATDC position.

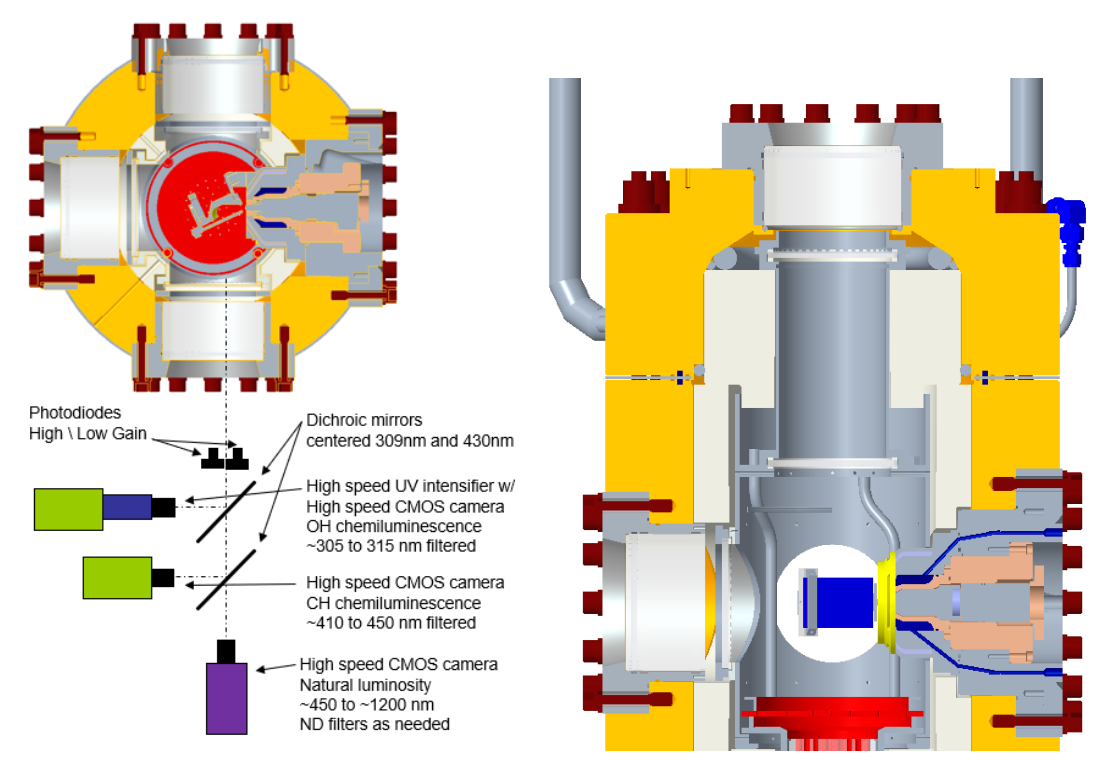


Fig. 4. High Temperature Pressure Vessel experimental and optical setup



Fig. 5. Physical 3D-Piston Setup

Four high-speed cameras and two photo diodes allowed for observation of the combustion during the interaction of the fuel-jet with the 3D piston section and glass cylinder head. One camera with a CH\* (430 nm ±20 nm) filter provided a profile view, and the other three cameras (NL, CH\*, OH\*) provided a top view of the piston bowl through the transparent cylinder head as shown in Fig. 4.

The HTPV was operated with an ambient pressure of 120 bar for all testing, corresponding approximately to cylinder pressure at start of combustion (SOC) for the engine testing. The ambient flow was 40 m<sup>3</sup>/h with 18% O<sub>2</sub> concentration. Testing of the 3D piston sections was accomplished by varying ambient temperature, injection pressure, and injection duration as shown in Table 4 below. The final bowl profile for the TBC coated piston differs slightly from the production bowl profile targets as shown in Fig. 3. Detailed analysis is focused on the 975 K, 200 MPa, and 840 µs condition targeting a hydraulic injection duration of 1900 µs.

A single-orifice on-axis fuel injector was used in the HTPV. The orifice diameter was 239 µm which was the closest single-orifice available to the engine injector orifice diameter. Because of it having a singleorifice fuel injector tip, the rate shape was very square with little front-end ramp.

Temperature (K)	Injection pressure (MPa)	Injection duration (µs)
875	100	410 - 1050
875	200	340 - 840
975	100	410 - 1050
975	200	340 - 840

Table 4. Summary of HTPV test conditions.

## 2.4 Engine Operating Conditions

In an effort to evaluate the benefits of TBC piston over standard steel piston, high load settings at various engine speeds were selected as shown in Table 5 below.

Engine Speed	rpm	2100	2100	1800	1800	1425	1425
EGR	%	18	0	20	0	14	14
Fueling	g/min	317	317	231	231	265	209
Rail Pressure	MPa	250	160	180-220	140-180	160	180-220
Torque	N-m	361-427	356-416	297-373	315-375	486-532	387-434
Inj Duration	° (deg)	19.9	25.8	15.2-17.4	17.3-20.2	21.3	13.8-15.5
Intake Temp	°C	66	50	59	50	53	63
Intake Pres	kPa-a	362	333	334	298	411	287
Exhaust Pres	kPa-a	419	433	389	349	468	310

Table 5. Engine Test Conditions

These test settings are representative of typical EGR levels in various engine applications and existing state of art turbochargers on heavy duty diesel engines. At each test condition, the full range of engine operation was realized by changing injection timings to achieve peak cylinder pressure and to stay within the end of injection limit at constant fueling.

Data point 2 in Table 6 below has been used in the detailed analysis of steel and TBC pistons.

Data Point		2	2	2
Piston		Steel	Steel (Repeat)	TBC
Engine Speed	rpm	1800	1800	1800
EGR	%	20	20	20
Fueling	g/min	231	231	231
Rail Pressure	MPa	220	220	220
Torque	N-m	353	355	347
Start of Injection	° crank angle (ATDC)	-1.85	-1.7	-1.71
End of Injection	° crank angle (ATDC)	13.38	13.58	13.56
Injection Duration	° crank angle	15.23	15.28	15.28
Intake Runner Temperature	°C	59	59	59
Intake Runner Pressure	kPa-a	334	334	334
Exhaust Runner Pressure	kPa-a	389	389	389

Table 6. Test Data - Steel vs. TBC Piston

# 3. Results and Analysis

## 3.1 Single Cylinder Test Engine

A detailed view of the in-cylinder combustion processes is shown in Fig. 6 for the second SOI timing point at an 1800 rpm 1900 kPa IMEPn mode. The steel piston and TBC piston cases are shown with a repeat of the steel piston. The lower pressure of the TBC case is attributed to a slightly lower measured geometric compression ratio of 16.77 vs. 16.98 and a slightly lower pressure at IVC for the same nominal IMAP boundary condition. Ideally the compression pressure would be better matched, but the authors do not believe this variance impacts the result trends significantly. Evidence toward this is the repeat steel piston case which has good peak heat release rate consistency despite cylinder pressure variance originating from simply rebuilding the engine and remeasuring.

Differences in heat release rates can be seen with the TBC piston having lower peak rates in the apparent heat release rate (AHRR) plot and a slower 50-90% burn in the cumulative AHRR plot. A slower fuel-air mixing system can be inferred from these immediate heat release observations, but some further analysis rigor can help with detailed and fair comparisons. A useful parameter which consolidates the impact of the heat release rate, duration, shape and phasing in the cycle is the Heat Release Rate Efficiency in (Eqn. 1) and is similar to other calculations of degree of constant volume combustion [19] or effective expansion ratio 20].

Heat Release Rate Efficiency = 
$$\frac{\int_{soc}^{eoc} \frac{dQ}{d\theta} \eta_{otto(\theta)} d\theta}{\int_{soc}^{eoc} \frac{dQ}{d\theta} d\theta}$$
 (Eqn. 1)

This utilizes a simple Otto cycle efficiency calculation of the instantaneous expansion ratio  $(V_{max} / V(\theta))$  in (Eqn. 2),

$$\eta_{otto(\theta)} = 1 - \frac{1}{\left(\frac{V_{max}}{V(\theta)}\right)^{V-1}}$$
(Eqn. 2)

where  $\gamma$  is the ratio of specific heats computed from the heat release analysis. Integration of the heat release dQ/d $\theta$  weighted Otto cycle efficiency, over the combustion duration from SOC to end of combustion (EOC), provides a single metric to compare and contrast engine cycles with heat release, compression ratio, and expansion ratio variation. This heat release rate efficiency will be used for comparisons in the following figures.

The difference between the fuel input energy and the cumulative AHRR, at the end of the closed cycle, in Fig. 6 is shown and is one way to define the in-cylinder heat transfer. Between the three cases there are differences in this heat transfer metric, but it is small and susceptible to the quality of the cylinder pressure measurement. Further plots in Fig. 7 and Fig. 8 compare larger data sets and differences.

Fig. 7 shows the emissions and engine performance comparisons for the timing sweep which includes point #2 from Table 6 and Fig. 6. The TBC piston has a slightly shifted-left NOx/ISFC response, which is expected due to the slower heat release rates, and it produces the highest particulate. CO emissions go generally with the particulate emissions while hydrocarbon emissions are very low for all cases. The volumetric efficiency of the TBC piston is the lowest and indicates a charge air heating phenomena classic to the historical TBC efforts in diesel engines. The tighter collapse of the ISFCn plotted against heat release rate efficiency, compared to when it is plotted against CA50, shows the usefulness of this method for normalization – clearly no efficiency benefit is observed for the TBC piston.

The final two plots in Fig. 7 attempt to describe the differences in heat transfer with the in-cylinder heat transfer metric previously described, and a direct measurement of oil heat rejection through oil flow and oil temperature increase. The TBC piston in-cylinder heat transfer goes between the two steel piston data sets with a flatter trend with SOI/CA50. However, the TBC piston oil heat rejection matches the steel piston repeat data set very closely. The lower steel piston oil heat rejection, relative the repeat steel piston, was a result of a misaligned piston cooling oil jet and the discovery of produced the need for the repeated steel piston data. This provides a useful discussion point in that if this magnitude of oil heat rejection reduction from a cooling system modification could not produce measurable efficiency differences, similar reductions in heat transfer from a TBC likely would also not produce measurable efficiency differences. The caveat here being that the actual surface temperature change or "swing" from the TBC should be larger than that imposed by a simple cooling change, and theoretically (by 0D

and 3D models) should be able to reduce heat transfer more effectively. A lack of sufficient experimental TBC surface temperature understanding confounds this issue. A final point is that only adding thermal resistance to one of the multiple in-cylinder heat transfer paths/surfaces (i.e., just the piston) may be insufficient to significantly reduce or change the total heat transfer, as the heat may find other less resistive paths.

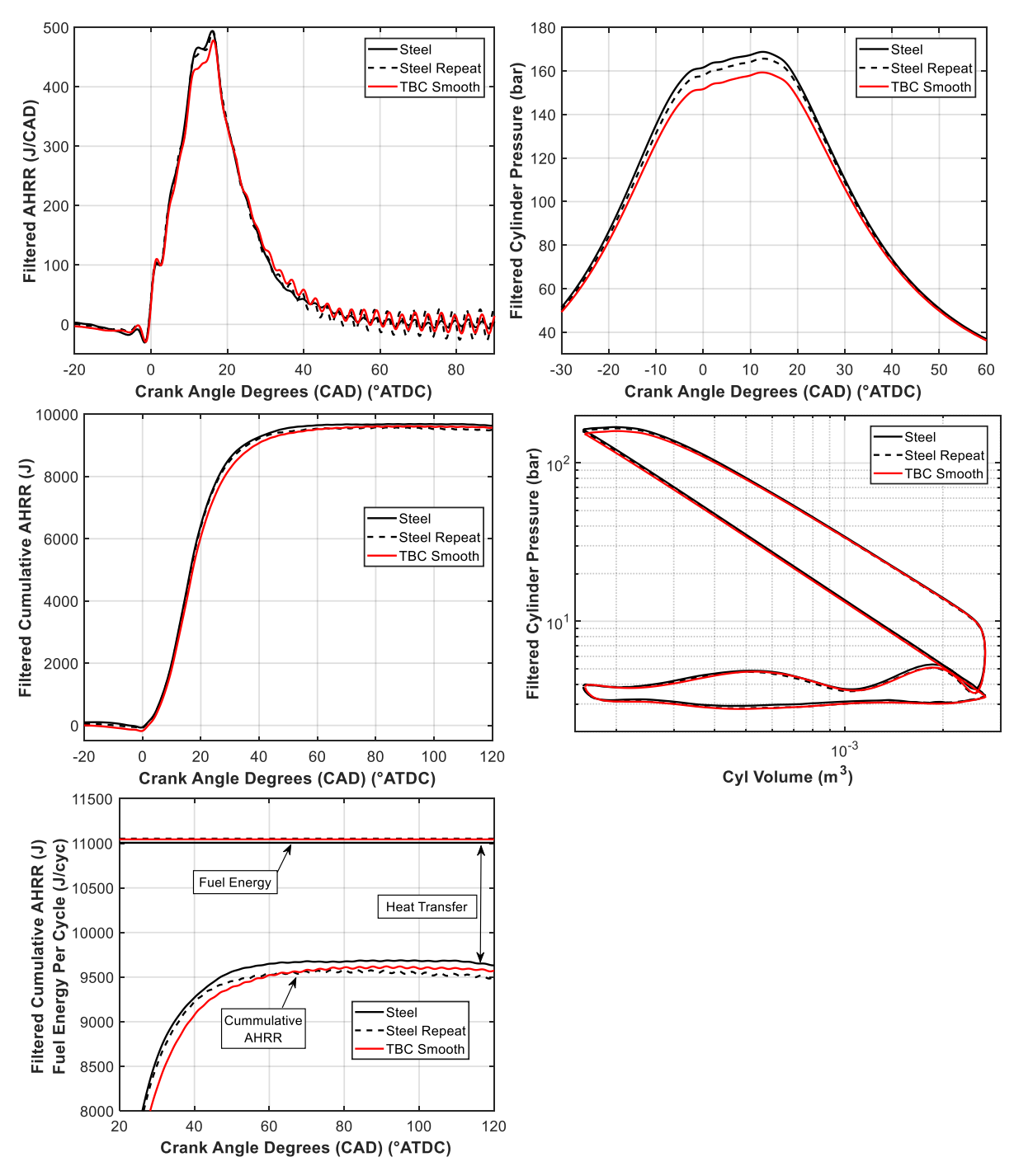


Fig. 6. SOI Point#2 from Table 6, 1800 rpm, 231 g/min fueling (nominally 1900 kPa IMEPn), 24.5 AFR, 20% EGR, 220 MPa rail pressure high-speed data

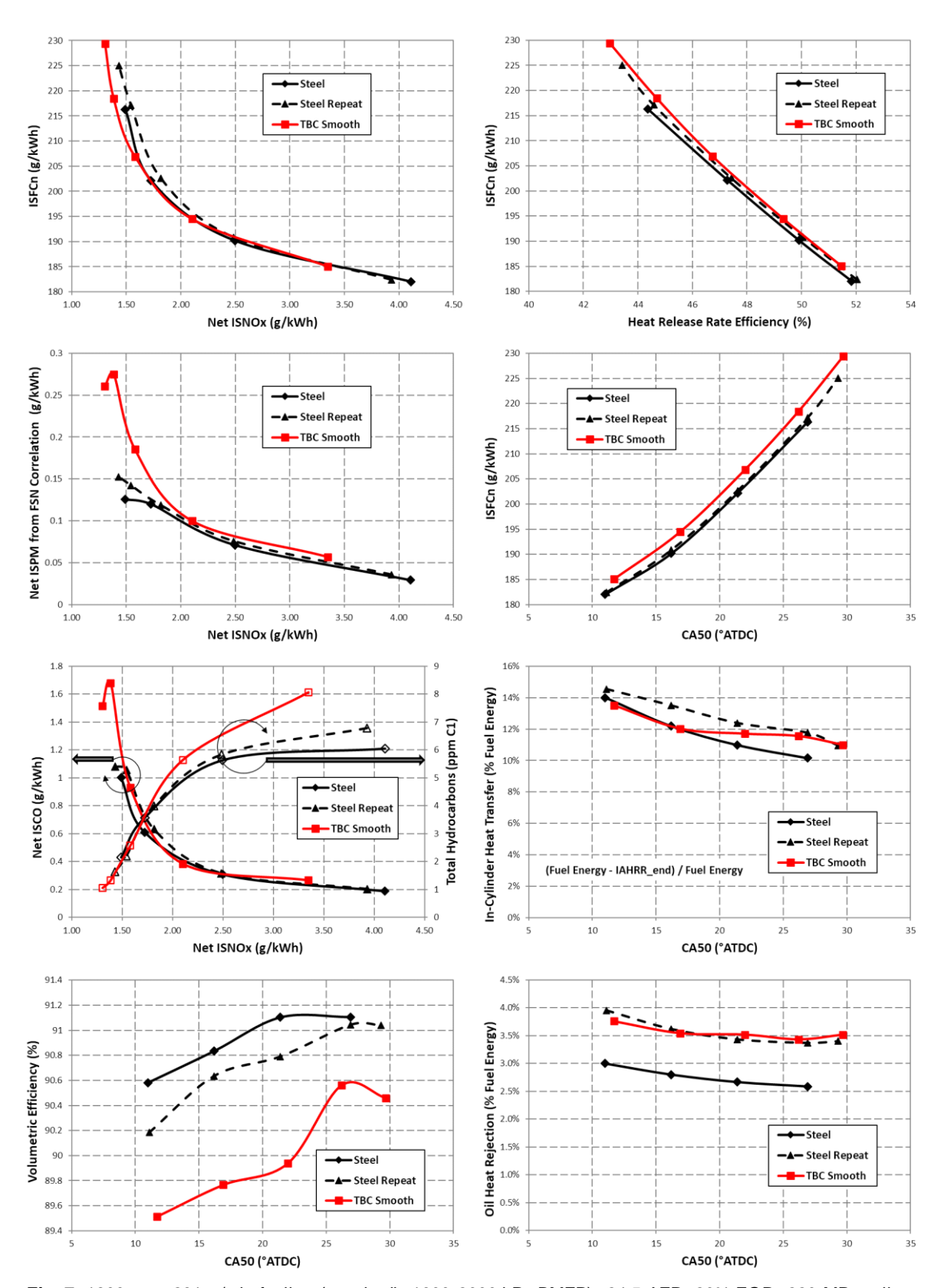


Fig. 7. 1800 rpm, 231 g/min fueling (nominally 1600-2000 kPa BMEP), 24.5 AFR, 20% EGR, 220 MPa rail pressure, timing sweep low-speed data

The data plotted in Fig. 8 attempts to provide a macroscope view of the general efficiency and heat loss trends from the present single cylinder engine experimental campaign. All the comparable data between the steel (repeat) piston and TBC piston are overplotted and show very similar trends and scatter. The in-cylinder heat transfer plot agrees with the data for oil and total heat rejection, and these are not shown

for brevity. Fig. 8 solidifies the conclusion that there was no obvious fuel consumption or heat transfer differences confidently observed and motivated the need toward further fundamental investigation into combustion system differences imposed by the addition of the TBC piston surface. It should be noted that there are a small number of points, similar to Fig. 6 and Fig. 7, where a possible heat transfer reduction could be argued, but the overwhelming trend is one of similar heat transfer for a given heat release efficiency. Toward this fundamental understanding, the following sections will discuss the optical efforts in the high temperature pressure vessel.

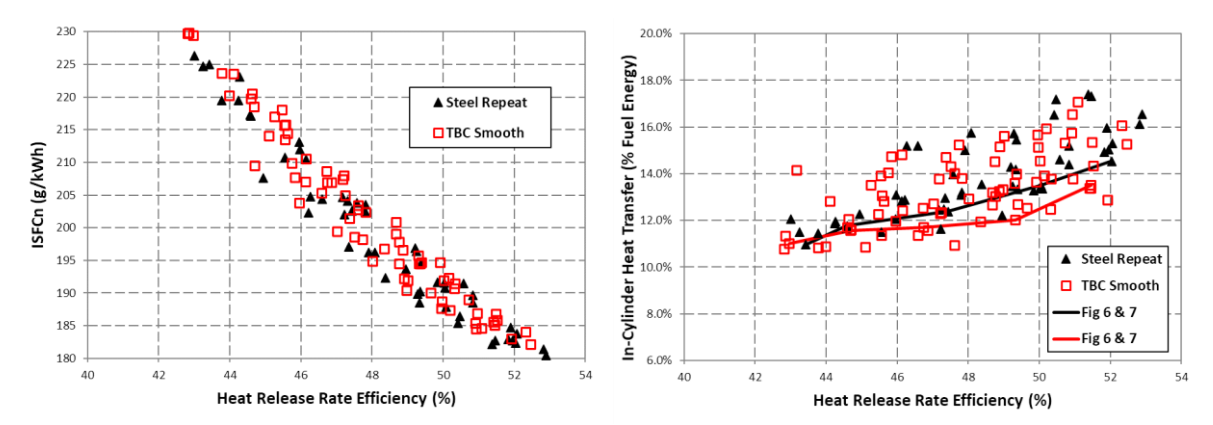


Fig. 8. All comparable operating points (1425-2100 rpm and 1500-2800 kPa IMEPn) showing no obvious fuel consumption (ISFCn) or macroscopic heat transfer difference between the steel and TBC pistons in the SCTE.

#### 3.1 High Temperature Pressure Vessel

Fig. 9 shows an alignment image from the TCH\* camera where the single-orifice fuel injector tip is on the left and the 3D piston section is rotated such that the fuel jet mimics a 130 deg included angle. The 3D piston section is located 2 mm below the TDC position, which is the 10 CAD BTDC/ATDC position to represent a 20 CAD time window. A fused silica window, seen above the 3D piston section, represents the cylinder head positioned correctly relative to the fuel jet.

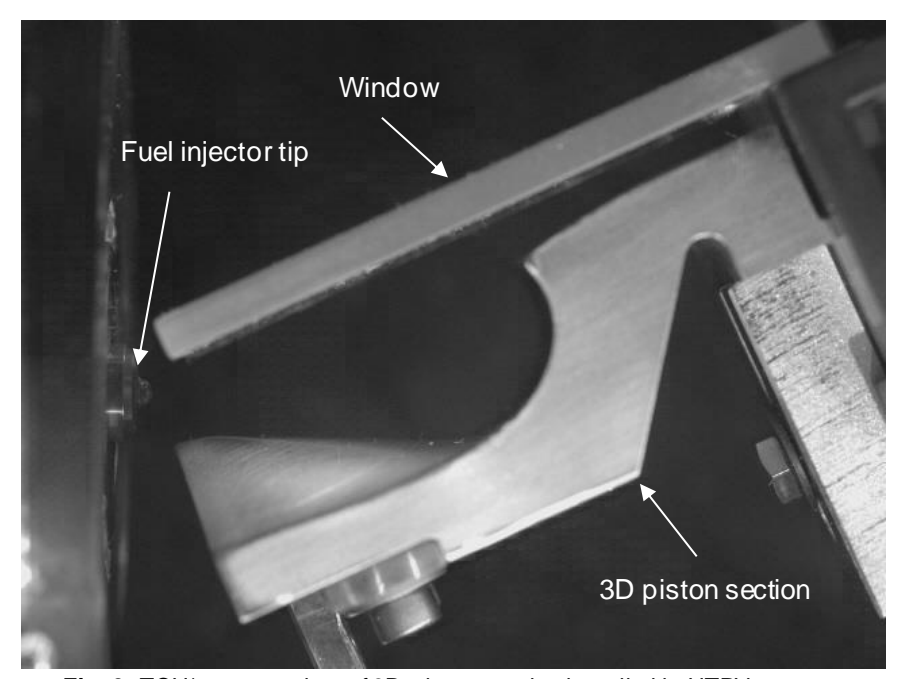


Fig. 9. TCH\* camera view of 3D piston section installed in HTPV

Fig. 10 shows the image in Fig. 9 after it has been masked and false-colored according to light intensity. The mask generated from the alignment image is then applied to all images taken with that hardware setup. The masking reduces CIV processing time, improves the CIV results, and it makes it easier to view the CIV results.

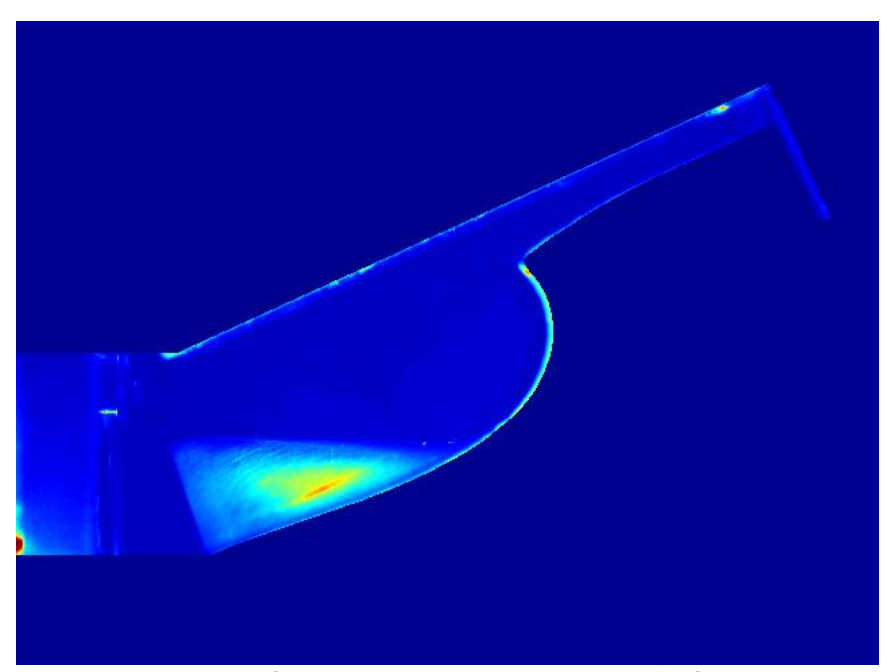


Fig. 10. False-colored TCH\* camera view with mask applied for CIV processing

Fig. 11 shows a sequence of averaged raw images from the TCH\* camera where the ambient temperature is 975 K, the injection pressure is 200 MPa, and the commanded injection duration is 840 µs. The false-color scaling is the same for all images and each image shows an average of four injections. The left column shows the metal piston, and the right column shows the smooth TBC piston. The columns are time aligned where the inserted text shows the time after start of injector current. The first time is when the flame front has come out of the piston bowl, has filled the squish region, and is starting to move back toward the injector along the cylinder head. The second time is when the flame is moving along the head toward the injector, and it is also starting to escape the volume between the piston and the window indicating that it is the time of jet-jet interaction. The third time is when the flame front is very near the lift-offlength, and it can be clearly seen that the flame in the metal piston has moved closer to the injector. This is due to the more rounded piston bowl lip that the smooth piston has. The fourth time is at end of injection. The flame in the metal piston bowl exhibits a brighter flame consistently, which may be another indication of faster mixing.

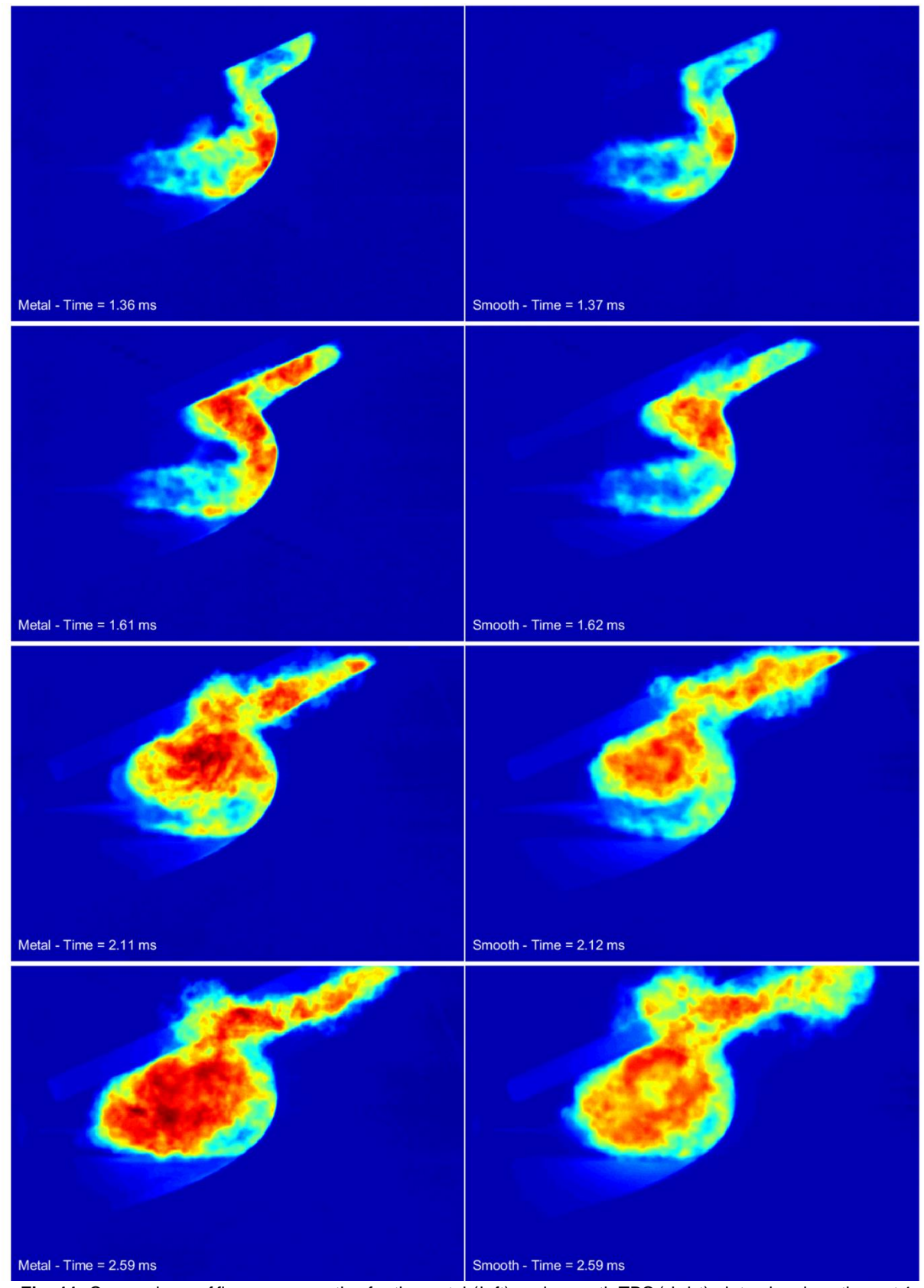


Fig. 11. Comparison of flame propagation for the metal (left) and smooth TBC (right) piston bowl sections at 4 times. Each image is an average of 4 shots. 975 K, 200 MPa,  $840~\mu s$ .

### 3.3 CIV image processing

Particle Imaging Velocimetry techniques were used to process the combustion images even though no seed particles were used. The assumption was that the sooty, bright flame envelope would have distinctive spots that would move from one image to the next and that the PIV code could track those, hence Combustion Imaging Velocimetry (CIV). The groundwork for CIV in optical engines was laid with Dembinski et al. [21-22] and expanded and proliferated by others such as Zha and Busch et al. [23-24] It should be noted that under these conditions, using a 239 µm orifice, the flame is optically thick. This means that the camera images the first surface closest to the camera, and therefore the CIV processing is based on the edge of the flame. The freely available MATLAB code PIVIab was used [25].

The raw high speed TCH\* movies were pre-processed in MATLAB before being imported into PNIab. The pre-processing consisted of applying a mask, a sharpening filter, and then the intensity was stretched from the movie minimum to the movie maximum intensity values. The sharpening and the intensity stretching was done to maximize contrast. Finally, it was saved in the MPEG4 format which could be imported into PIVIab.

Fig. 12 show plots of the mean correlation coefficients and the mean of correlation coefficients greater than 0.5 as a function of time for the metal and smooth piston bowl sections. The plots are a good representation for other operating points. This suggests that there is good confidence in the velocity results from the CIV image processing. The regularly appearing outliers (every 0.5 ms) are artifacts of the processing and should be ignored.

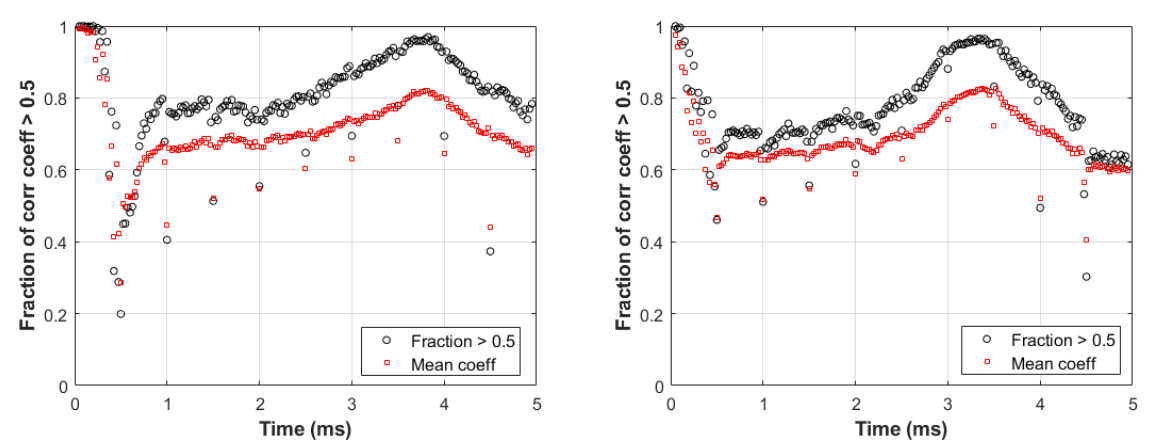


**Fig. 12.** Correlation coefficients for the metal (left) and smooth TBC (right) piston bowls at 975 K, 200 MPa, 840 us. In general representative for all cases.

Fig. 13 shows a calculated velocity field from CIV image processing at time 2.1 ms at 975 K, 200 MPa, 840 µs. The velocity field is calculated from shot 1 and is superimposed on a false-colored image from shot 1. When displaying the velocity field, a moving average in time was also applied to smooth it out and make it look more consistent. There is a very clear vortex and a clockwise rotation. Peak velocities reach about 60 m/s for the 200 MPa injection pressure. The vortex forms when the flame front reaches the cylinder head and lasts until the flame is burned out.

Pastor et al. [26] proposed a numerical method using the curl of the velocity field to locate the center of the vortex. This method was applied to the CIV velocity field in the hope of tracking the vortex center in time but did unfortunately not yield a good result for this data.

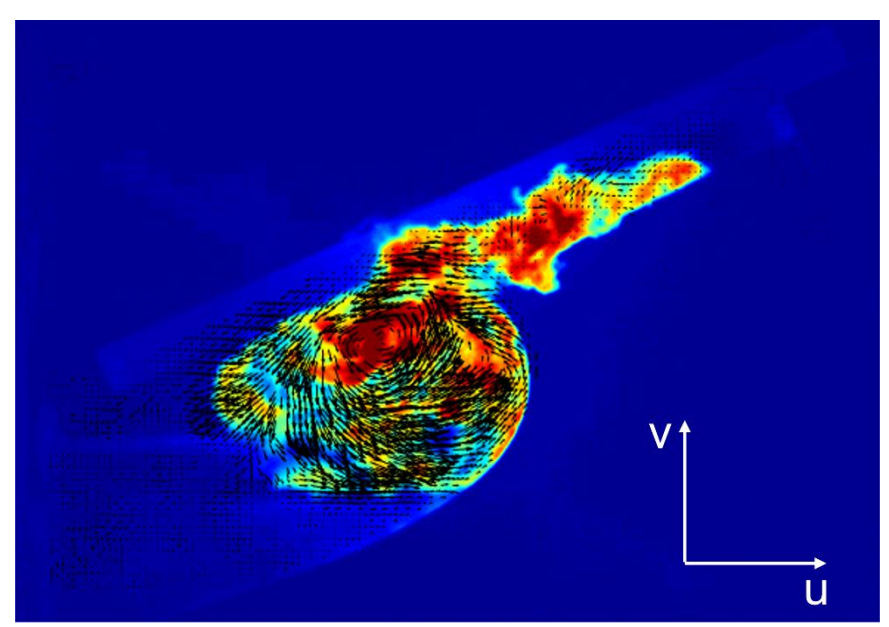


Fig. 13. Velocity field superimposed on false-colored TCH\* image of individual shot at 975 K, 200 MPa, 840 µs. Metal piston at 2.1 ms after start of injector current.

While the flame clearly expands along the piston bowl in the azimuthal direction (in and out of the image). most of the momentum is in the direction of the spray. Therefore, it is assumed that the majority of the momentum is illustrated by the two-dimensional velocity field shown in Fig. 13. From this idea the apparent chamber mixing energy in the velocity field can be calculated as shown below in Egn. 3.

Apparent chamber mixing energy = 
$$\sum_{i=1}^{1} (u^2 + v^2)$$
 (Eqn. 3)

Fig. 14 shows the calculated apparent chamber mixing energy and its u and v components for the metal and smooth piston sections as a function of time. The apparent chamber mixing energy is only calculated inside the masked area. The u component is clearly larger which makes sense since that is the direction of the fuel jet. It is also clear that the metal piston exhibits a greater mixing energy, mostly due to the faster penetration in the u direction as the v components are very similar. This is numerical evidence of the brighter flame which was visually seen in Fig. 11.

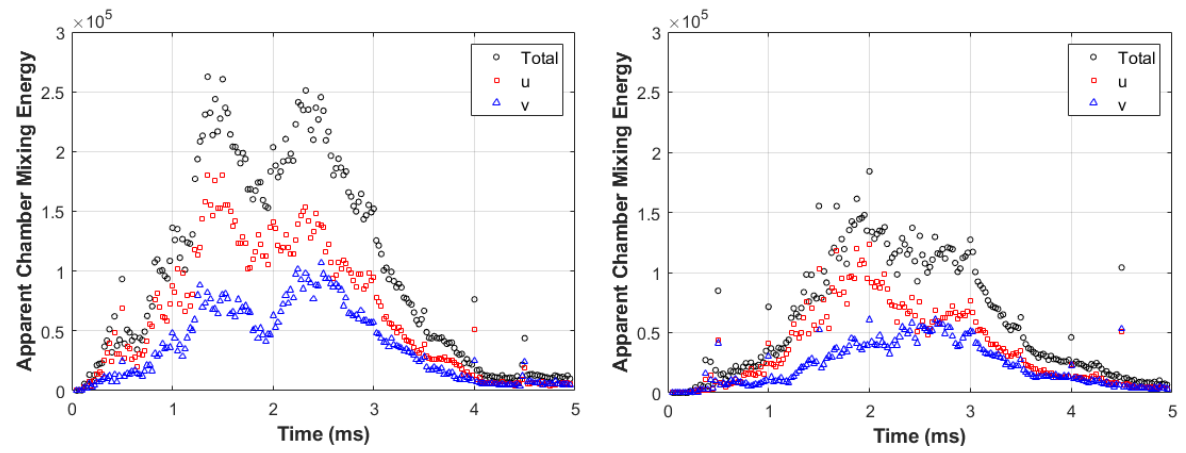


Fig. 14. Apparent chamber mixing energy for the Metal (left) and Smooth (right) piston bowl sections at 975 K, 200 MPa, and 840 µs.

Fig. 15 and Fig. 16 show side by side comparisons between metal and smooth for the lower injection pressure of 100 MPa, and a shorter duration of 355 µs. Note that the scales are the same for all 6 plots. One variable at a time is varied from the focus case of 975 K, 200 MPa, and 840 µs. The comments for Fig. 15 generally are true for Fig. 15 and Fig. 16. Note that the lower injection pressure of 100 MPa shown in Fig. 16 also shows a lower apparent chamber mixing energy.

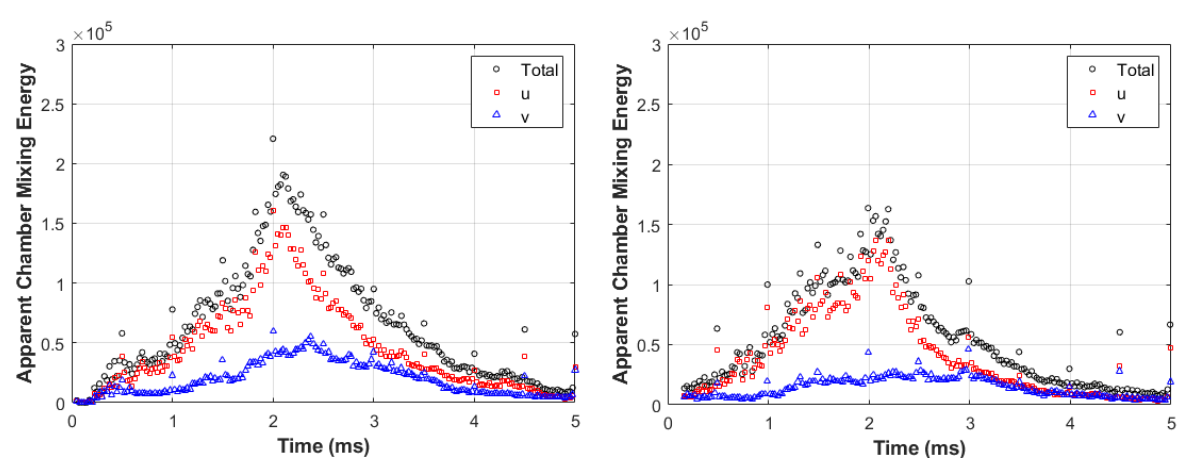
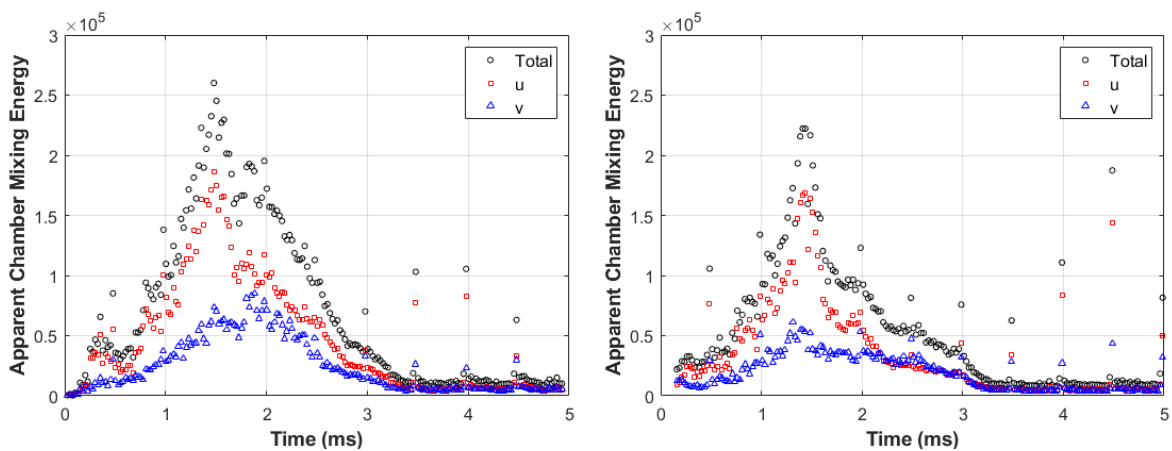


Fig. 15. Apparent chamber mixing energy for the Metal (left) and Smooth (right) piston bowl sections at 975 K, 100 MPa, and 1050 µs.



**Fig. 16.** Apparent chamber mixing energy for the Metal (left) and Smooth (right) piston bowl sections at 975 K, 200 MPa, and 355 μs.

#### Conclusions

In the present effort to measure and understand the impact of adding a TBC to a diesel engine piston the following conclusions were found. These were obtained using single cylinder engine testing and optical imaging diagnostics in a continuous flow high temperature pressure vessel.

- High-load engine performance, combustion and emissions measurements between a steel and a
  smoothed TBC (YSZ-type coating) piston showed the TBC piston had slower heat release rates,
  elevated PM and CO at retarded timings, and similar single digit ppm hydrocarbons. Comparing
  performance based on net ISNOx and Heat Release Rate Efficiency indicated that the smoothed
  TBC piston behaved like a slower mixing system with a naturally lower NOx response.
- No reduction in in-cylinder heat transfer or engine/piston oil heat rejection could confidently be
  measured at times with normalized heat release performance. Repeat measurements of the steel
  piston indicate the variability of the physical SCTE hardware and measurement system is significant, in the same range as the desired TBC heat transfer benefits and adds difficulty for comparisons between low repetition testing campaigns.
- The piston bowl corner feature, radius, and fine geometry are known to be critical to the mixingcontrolled combustion system performance. The TBC coating process was not able to achieve the precise corner and reentrancy geometry and is the primary aspect attributed to the deteriorated system fuel-air mixing.

- The 3D-piston section test concept for optical vessels was found to be very useful for understanding flame development in the combustion chamber, albeit with limitations. It is also believed to have produced useful data for future simulation validation efforts.
- The rounded piston bowl rim for the smooth TBC case slows the flame development and reduces the mixing energy, as seen in the HTPV results, and explains the slow heat release rate in the engine case. The mechanism for reduced fuel-air mixing was found to be the rounder bowl corner and reduced corner reentrancy which produced weaker mixing vortices with lower momentum.
- The concept of apparent chamber mixing energy was introduced through CIV methods. It was found to capture the effect of the rounded bowl edge sufficiently, and it also captured impact of iniection pressure.
- The 3D-piston section test concept, with analyses such as CIV, can give an experimental understanding of the combustion and flame development changes to a mixing-controlled combustion system due to perturbations such as a TBC surface. The importance of understanding the combine system impact should be highlighted, as the system is highly refined and there are interactions which can offset and hide the desired outcome or result.

After reviewing the present work and discussing with team members, the following steps are proposed to further the research and development on both the 3D-piston diagnostic and TBC for engine efficiency.

- Employ the 3D-piston section test concept to other combustion system topics and questions of interest.
- Simulate the HTPV results with CFD to determine the magnitude of importance for the different surface roughness – and use this data for CFD simulation validation.
- Produce steel variants of the pistons matching the as-produced TBC bowl shapes so further testing can eliminate the differences in bowl geometry.
- Gain fundamental surface temperature and heat flux data to understand what the true impact of the TBC is on heat transfer and the near-wall temperature gradient.

#### **Acknowledgements**

This research was conducted with funding from the U.S. Department of Energy, Office of Energy Efficiency and Renewable Energy, Vehicle Technologies Office, under the award DE-EE0008476. Many people from the Caterpillar Technical Center in Mossville IL, USA contributed to aspects of this work. The authors would like to thank Justin Sedekum for assisting in the engine operation, and Jeremy Adams for the design of the engine and optical components for manufacturing. For discussions on TBC testing and engine performance the authors are grateful for Jason Rasmussen's input and insight. Lastly, the team would like to thank Dan Sordelet for his thermal spray and materials science expertise, input, and guidance throughout the research.

#### References

- 1. Kosaka, H., Wakisaka, Y., Nomura, Y., Hotta, Y. et al., "Concept of "Temperature Swing Heat Insulation" in Combustion Chamber Walls, and Appropriate Thermo-Physical Properties for Heat Insulation Coat," SAE Int. J. Engines 6(1):142-149, 2013, https://doi.org/10.4271/2013-01-0274.
- 2. Uchida, Noboru. "A Review of Thermal Barrier Coatings for Improvement in Thermal Efficiency of Both Gasoline and Diesel Reciprocating Engines." International Journal of Engine Research 23, no. 1 (January 2022): 3-19. https://doi.org/10.1177/1468087420978016
- Wakisaka, Y., Inayoshi, M., Fukui, K., Kosaka, H. et al., "Reduction of Heat Loss and Improvement of Thermal Efficiency by Application of "Temperature Swing" Insulation to Direct-Injection Diesel Engines, "SAE Int. J. Engines 9(3):1449-1459, 2016, https://doi.org/10.4271/2016-01-0661.
- 4. Kawaguchi, A., Wakisaka, Y., Nishikawa, N., Hidemasa Kosakaet, H., et al. "Thermo-Swing Insulation to Reduce Heat Loss from the Combustion Chamber Wall of a Diesel Engine" International Journal of Engine Research 20, no. 7, September 2019: 805-16. https://doi.org/10.1177/1468087419852013.

- 5. Binder, C., Abou Nada, F., Richter, M., Cronhjort, A. et al., "Heat Loss Analysis of a Steel Piston and a YSZ Coated Piston in a Heavy-Duty Diesel Engine Using Phosphor Thermometry Measurements," SAE Int. J. Engines 10(4):1954-1968, 2017, https://doi.org/10.4271/2017-01-1046.
- 6. Witkowski, D., Rothamer, D.A., "Precise surface temperature measurements from 400 to 1200 K using the Pr:YAG phosphor," Appl. Phys. B 127, 171 (2021). https://doi.org/10.1007/s00340-021-07723-5
- 7. Andrie, M., Kokjohn, S., Paliwal, S., Kamo, L. et al., "Low Heat Capacitance Thermal Barrier Coatings for Internal Combustion Engines," SAE Technical Paper 2019-01-0228, 2019, https://doi.org/10.4271/2019-01-0228.
- 8. Andruskiewicz, P., Najt, P., Durrett, R., and Payri, R., "Assessing the Capability of Conventional In-Cylinder Insulation Materials in Achieving Temperature Swing Engine Performance Benefits" International Journal of Engine Research 19, no. 6, August 2018: 599–612. https://doi.org/10.1177/1468087417729254.
- 9. Hazhizume, T., Tanno, S., Mori, S., Yoshihara, Y. "Study of the Heat Transfer in the Spark-ignited Engines for Reducing Heat Loss," JSAE Transaction 53(1):107-113, 2022. https://www.jst-age.jst.go.jp/article/jsaeronbun/53/1/53\_20224041/\_pdf
- Broatch, A., Olmeda, P., Margot, X., Gomez-Soriano, J. "Numerical simulations for evaluating the impact of advanced insulation coatings on H2 additivated gasoline lean combustion in a turbocharged spark-ignited engine," Applied Thermal Engineering 148 (2019): 674-683. https://doi.org/10.1016/j.applthermaleng.2018.11.106.
- 11. Broatch A., Olmeda P., Margot X., Gomez-Soriano, J. "A one-dimensional modeling study on the effect of advanced insulation coatings on internal combustion engine efficiency," International Journal of Engine Research 22(7):2390-2404, 2021, doi:10.1177/1468087420921584
- 12. Gingrich, E., Tess, M., Korivi, V., Schihl, P., et al. "The Impact of Piston Thermal Barrier Coating Roughness on High-Load Diesel Operation." International Journal of Engine Research, December 2019, https://doi.org/10.1177/1468087419893487.
- 13. Somhorst, J., Oevermann, M., Bovo, M., and Denbratt, I., "Evaluation of Thermal Barrier Coatings and Surface Roughness in a Single-Cylinder Light-Duty Diesel Engine" International Journal of Engine Research, October 2019, https://doi.org/10.1177/1468087419875837.
- 14. Koutsakis, G., Saputo, J., Gingrich, E., Tess, M. et al., "Delamination Failure on High-Output Diesel Engine Thermal Barrier Coatings," SAE Technical Paper 2022-01-0440, 2022.
- 15. Koutsakis, G., and Ghandhi, J.B. "Analytical solution of unsteady heat conduction in multilayer internal combustion engine walls," Applied Thermal Engineering 213 (2022): 118681. https://doi.org/10.1016/j.applthermaleng.2022.118681.
- 16. Kawaharazuka, F., Uchida, N., and Osada, H., "A Novel Piston Insulation Technique to Simultaneously Improve Both Heat Loss and Thermal Efficiency for Diesel Engines," SAE Int. J. Adv. & Curr. Prac. in Mobility 3(5):2173-2181, 2021, https://doi.org/10.4271/2021-01-0453.
- 17. Svensson, K. and Martin, G., "Ducted Fuel Injection: Effects of Stand-Off Distance and Duct Length on Soot Reduction," SAE Int. J. Adv. & Curr. Prac. in Mobility 1(3):1074-1083, 2019, https://doi.org/10.4271/2019-01-0545.
- 18. Svensson, K. and Martin, G., "Improved Method for Studying MCCI Flame Interactions with an Engine Combustion Chamber," SAE Technical Paper 2021-01-0507, 2021, doi:10.4271/2021-01-0507.
- 19. Shudo, T, S Nabetani, and Y Nakajima., "Analysis of the Degree of Constant Volume and Cooling Loss in a Spark Ignition Engine Fuelled with Hydrogen," International Journal of Engine Research 2(1): 81–92, 2001, https://doi.org/10.1243/1468087011545361.
- Stanton, D., "Systematic Development of Highly Efficient and Clean Engines to Meet Future Commercial Vehicle Greenhouse Gas Regulations," SAE Int. J. Engines 6(3):1395-1480, 2013, https://doi.org/10.4271/2013-01-2421.
- 21. Dembinski, H., Angstrom, H., and Razzaq, H., "In-Cylinder Flow Pattern Evaluated with Combustion Image Velocimetry, CIV, and CFD Calculations during Combustion and Post-Oxidation in a HD Diesel Engine," SAE Technical Paper 2013-24-0064, 2013, https://doi.org/10.4271/2013-24-0064.
- 22. Dembinski, H.W.R., "The Effects of Injection Pressure and Swirl on In-Cylinder Flow Pattern and Combustion in a Compression-Ignition Engine," International Journal of Engine Research 15(4):444-459, 2014, doi:10.1177/1468087413491262.

- 23. Zha, K., Busch, S., Warey, A., Peterson, R. et al., "A Study of Piston Geometry Effects on Late-Stage Combustion in a Light-Duty Optical Diesel Engine Using Combustion Image Velocimetry." SAE Int. J. Engines 11(6):783-804, 2018, https://doi.org/10.4271/2018-01-0230.
- 24. Busch, S., Park, C., Warey, A., Peterson, R. et al., "A Study of the Impact of Pilot-Main Dwell on Late-Cycle Flow in the Piston Bowl of a Light Duty Optical Diesel Engine," 12th International Symposium on Combustion Diagnostics, May 10-1, Baden-Baden, Germany, 2016. https://www.osti.gov/servlets/purl/1367016
- 25. Thielicke, William, and René Sonntag. "Particle Image Velocimetry for MATLAB: Accuracy and Enhanced Algorithms in PIVIab." Journal of Open Research Software, vol. 9, Ubiquity Press, Ltd., 2021. doi:10.5334/iors.334.
- 26. Pastor, J.V., Garcia-Oliver, J.M., and Pachano, L. "Evaluation of Vortex Center Location Algorithms for Particle Image Velocimetry Data in an Optical Light-Duty Compression Ignition Engine," SAE Technical Paper 2018-01-0209, 2018.